

---

# NON-TRIVIAL TOPOLOGICAL PHASE IN THE $\text{Sn}_{1-x}\text{In}_x\text{Te}$ SUPERCONDUCTOR

---

A PREPRINT

**Tome M. Schmidt**Instituto de Física, Universidade Federal de Uberlândia,  
Uberlândia, Minas Gerais 38400-902, Brazil**G. P. Srivastava**School of Physics, University of Exeter,  
Stocker Road, Exeter EX4 4QL, UK

November 18, 2021

**ABSTRACT**

Whereas SnTe is a inverted band gap topological crystalline insulator, the topological phase of the alloy  $\text{Sn}_{1-x}\text{In}_x\text{Te}$ , a topological superconductor candidate, has not been clearly studied so far. Our calculations show that the  $\text{Sn}_{1-x}\text{In}_x\text{Te}$  band gap reduces by increasing the In content, becoming a metal for  $x > 0.1$ . However, the band inversion at the fcc L point for both gapped and gapless phases has been maintained. Furthermore, the computed topological invariant shows a non-trivial phase with a mirror Chern number  $n_M = -2$  for In concentrations of  $x = 0.03125$ ,  $x = 0.125$ , and  $x = 0.25$ . We also identify pairs of topologically protected states on the (001) surface of  $\text{Sn}_{1-x}\text{In}_x\text{Te}$  with  $\pm i$  mirror eigenvalues. The character of these topological states is affected by In dopant. As the In content  $x$  increases, the Dirac crossing point moves further away from the L point, and the Fermi velocity of the topological states increases significantly. Our results demonstrate a non-trivial topological phase for the superconductor  $\text{Sn}_{1-x}\text{In}_x\text{Te}$ , and provide a detailed description of the topological state properties.

**Keywords** topological crystalline insulator, topological superconductor, protected surface states**1 Introduction**

Topological phase of matter has received significant attention lately, starting from topological insulators (TIs) and more recently topological superconductors (TSCs) [1, 2, 3, 4, 5]. TIs are characterized by Dirac-like edge or surface states that can be protected by time reversal symmetry [6], or crystal lattice symmetry, the so called topological crystalline insulator (TCI) [7]. TSCs has special interest for potential quantum computing applications [5]. Topological superconductor phase has been proposed to be obtained through proximity induced by attaching a TI onto a conventional superconductor [8, 9], or by doping a TI turning it into a superconductor phase, like Cu, Sr or Nb doped  $\text{Bi}_2\text{Se}_3$  [10, 11, 12, 13, 14, 15, 16, 17, 18]. Recently, superconductivity has also been investigated by the doping of a TCI material, in particular In doped SnTe [19, 20, 21, 22, 23, 24, 25, 26, 27, 28, 29] or PbSnTe [30]. As SnTe is a TCI material [31, 32] and In doped SnTe is a superconductor,  $\text{Sn}_{1-x}\text{In}_x\text{Te}$  is expected to be a TSC material. Indeed,  $\text{Sn}_{1-x}\text{In}_x\text{Te}$  is a well characterized superconductor, whose critical temperature depends on the In doping rate, varying from  $T_C = 1.2 \text{ K}$  in low In doping regime [21] to  $T_C = 4.8 \text{ K}$  for higher In contents [24]. Although there is no doubt about the superconductivity phase, the preservation of its topological phase under In doping is a topic of current discussion. For low In concentration some experiments indicate a signature of topological surface states [21, 25], and recent experiments [33] show evidence of surface linear dispersion bands at high In doping rates. However, that does not confirm its topological order.

Also the superconductivity mechanism in  $\text{Sn}_{1-x}\text{In}_x\text{Te}$  is currently in discussion. Some previous experiments indicate that the superconductivity should be odd-parity pairing [19, 22], but more recently it has been attributed to a s-wave BCS model [23, 24, 27, 28]. Another intriguing question with respect to In doped SnTe TCI is its doping character. While low In concentrations generate hole-like doping, for high In doses it turns into electron-like carriers [26, 29]. The

hole-like can be expected, as In is a group III element substituted at a group IV atom, but no electron-like behaviour would be expected.

In this work we show that  $\text{Sn}_{1-x}\text{In}_x\text{Te}$  for In concentrations of  $x = 0.03125$ ,  $x = 0.125$  and  $x = 0.25$  the valence and conduction bands are inverted, giving a non-null Chern number. We have identified pairs of topological states protected by the mirror symmetry on the (001) surface of  $\text{Sn}_{1-x}\text{In}_x\text{Te}$  with opposite mirror eigenvalues  $\pm i$ . Our results show that the experimentally observed hole to electron carrier-like transition as a function of increased In concentration can be explained in terms of the depopulation of the In-5s orbital, which is pinned at the Fermi level. Furthermore, our results also indicate that  $\text{Sn}_{1-x}\text{In}_x\text{Te}$  is a  $s$ -wave superconductor.

## 2 Method

The mirror Chern number has been computed using the hybrid Wannier charge center scheme [34, 35], where the Wannier functions are constructed from first-principles calculations. The band structure and the projection of the mirror eigenvalues on the topological surface states have been computed using the density functional theory and generalized gradient approximation for the exchange and correlation functional [36]. Fully relativistic pseudopotentials within the projector augmented wave (PAW) scheme [37] have been used self-consistently within plane wave basis set with the kinetic energy cut-off of 340 eV. We used the Vienna Ab initio Simulation Package (VASP) for band structure and mirror projections [38, 39], and QUANTUM ESPRESSO [40] to compute the Wannier functions. Both SnTe and  $\text{Sn}_{1-x}\text{In}_x\text{Te}$  were modelled in the rock-salt structure. We used the experimental lattice parameter for SnTe, and following the lattice variation observed experimentally [22, 26] making a linear reduction of the lattice parameter for the In content compounds. The Brillouin zone (BZ) was sampled by using the Monkhorst-Pack special  $\mathbf{k}$ -points scheme [41], with grid-sizes as discussed later.

Calculations for bulk  $\text{Sn}_{1-x}\text{In}_x\text{Te}$  systems were performed by using a 64-atom cubic unit cell containing 32 cations (Sn/In) and 32 anions (Te) at the rock-salt basis sites. For  $x = 0, 0.03125, 0.125$  and  $0.25$  the number of In dopants per cell was 0, 1, 4 and 8, respectively. The BZ sampling was done with the  $(10 \times 10 \times 10)$  mesh of  $\mathbf{k}$ -points.

To compute surface states we modelled the  $\text{Sn}_{1-x}\text{In}_x\text{Te}$  system using two types of cells containing an atomic slab and a minimum of 15 Å of vacuum region. For  $x = 0$  (pristine SnTe) and  $x = 0.125$  we used a tetragonal cell with the atomic slab containing 128 and 64 atoms, respectively. For  $x = 0.125$  each slab in a tetragonal unit cell contained 4 In, 28 Sn and 32 Te atoms. For  $x = 0.03125$  we considered a cubic slab with 256 atoms (4 In, 124 Sn and 128 Te) in a unit cell. The BZ sampling for the cubic and tetragonal cells was done with  $(10 \times 10 \times 1)$  and  $(7 \times 7 \times 1)$   $\mathbf{k}$ -point meshes, respectively.

In order to discuss symmetry-related features in the band structure results for both bulk and slab geometries, we have presented a schematic sketch of a sample cubic cell of size  $a$  and of a sample tetragonal cell of base  $(a/\sqrt{2} \times a/\sqrt{2})$  on the left hand side of Fig. 1. On the right hand side of Fig. 1 we have shown the correspondence between the important BZ symmetry points for bulk (fcc) and their projection on the BZs for the cubic and tetragonal structures used in our modelling. In particular, we note that the bulk L points map onto the  $\bar{M}_c$  point of the cubic structure and onto the  $\bar{X}_t$  point of the tetragonal structure.

## 3 Results and Discussions

### 3.1 Topological Phase for In Doped Bulk SnTe

At room temperature SnTe has the simple rocksalt crystal structure. This IV-VI compound is a narrow-gap ( $E_g=0.18$  eV) semiconductor, with the conduction and valence band edges located at the four equivalent L points in the fcc BZ (two of which are marked in Fig. 1). In our modelling we chose to use the experimental lattice constant of 6.321 Å in order to facilitate comparison of electronic states in the gap region. In Fig. 2(a) we have plotted the electronic band structure of bulk SnTe using a simple cubic  $(2 \times 2 \times 2)$  unit cell (8 times the volume of the cubic cell in Fig 1) as mentioned in the Method section. The L point of the fcc BZ is folded onto the zone centre  $\bar{\Gamma}$  for this periodic structure. As shown in the bottom panel of Fig. 2(a) we obtain a band gap of 0.17 eV for bulk SnTe when the SO interaction is included.

In the absence of SO coupling, the VBM and CBM states at the L point in the BZ for IV-VI compounds are contributed by (s-cation, p-anion) and (s-anion, p-cation), respectively [42]. This is the expected normal ordering of the band edges in III-V and II-VI compounds [43, 44]. Due to relativistic interactions the cation/anion characters are inverted in SnTe, and the projected orbital contributions are  $\Phi_- = [\phi_P^{S^n} + \phi_S^{T^e}]$  (in orange) for VBM and  $\Phi_+ = [\phi_P^{T^e} + \phi_S^{S^n}]$  (in purple) for CBM. The Bloch eigenstates on the  $\Gamma$   $L_1$   $L_2$  plane in the fcc BZ are invariant under the mirror symmetry of rocksalt structure with respect to the family of  $\{110\}$  planes. The Bloch eigenstates for such mirror planes are also eigenstates

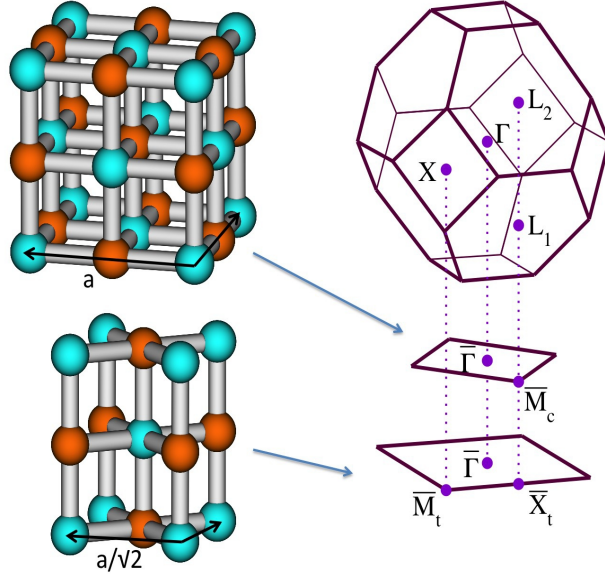


Figure 1: The rock-salt structures of SnTe modelled in this work. The panel on the left shows a sample cubic cell of size  $a$  and a sample tetragonal unit cell of base  $(a/\sqrt{2} \times a/\sqrt{2})$ . The panel on the right hand side shows the BZ for bulk (fcc) on the top, for the sample cubic structure in the middle, and for the sample tetragonal structure at the bottom. Note that the middle and bottom projections on the right hand side show  $(1 \times 1)/a$  and the  $(\sqrt{2} \times \sqrt{2})/a$  projected reciprocal unit cells.

of the mirror symmetry operator  $\mathcal{M}$ , with eigenvalues  $\pm i$ . For each class of Bloch eigenstates we compute the mirror Chern number using the Wannier charge center technique [45] obtaining  $n_M = -2$  in agreement with previous results [31, 32].

For  $\text{Sn}_{1-x}\text{In}_x\text{Te}$  the bulk conduction and valence bands edges (CBM and VBM) for  $x = 0.03125$ ,  $x = 0.125$  and  $x = 0.25$  are still inverted at the  $\bar{\Gamma}$ (L) point, as we can see in Fig. 2-(f)-(h). However for low In content  $x = 0.03125$  there is a clear total band gap, for higher In concentration it becomes a gapless system. Without the inclusion of spin-orbit interaction the conduction band dips inside the valence band, making  $\text{Sn}_{1-x}\text{In}_x\text{Te}$  metallic (see Fig. 2-(b)-(d)). This is in contrast to the pristine case ( $x = 0$ ), where there is still a very small gap between the VBM and CBM (Fig. 2-(a)) without the inclusion of the spin-orbit interaction.

For low In doping,  $x = 0.03125$ , we find an In state inside the bulk band gap and the Fermi level lies slightly below the valence band maximum (VBM) (see Fig. 2-(f)). This makes the system a gapped p-type doped semiconductor, in agreement with a recent study [26]. In order to understand the In effects we have highlighted (in pink) the In-5s contribution to the band structure (identified within the range -0.6 eV up to +0.5 eV) in Fig. 2(j). Some of these features are close to the  $\bar{\Gamma}$  point and some away from  $\bar{\Gamma}$  but close to  $E_F$ . However, close to the  $\bar{\Gamma}$  point there is a negligible In-5s contribution in the SnTe band gap region.

By increasing the In concentration to 12.5%, Fig. 2-(k), the In-derived levels go inside the valence band at the  $\bar{\Gamma}$  point. There is a clear development of In-5s related bands inside and across the band gap. More importantly, there are more significant (cf. larger symbols) In-5s contributions just below  $E_F$  across the BZ. Similarly for the high  $x$  regime of 25% of In, the metallic character is enhanced with more In-5s levels connecting valence and conduction bands as shown in Fig. 2-(l). It is interesting to note that there is a flat band originating from In-5s orbitals quite close to the Fermi level (around  $E_f - 0.054$  eV). For both  $x = 0.125$  and  $x = 0.25$  several In-5s bands are empty around  $E_F$ , with larger contributions for  $x = 0.25$ . This result can explain the transition from hole-like carriers in low In doping to electron-like carriers for higher In concentrations observed recently in experiments [29]. This transition can occur when the In-5s impurity level is partially occupied, turns it into  $\text{In}^{+3}$ , instead of the expected  $\text{In}^{+1}$  state. This  $p$ - to  $n$ -type transition has been found to occur even for a lower In concentration [26], which can be attributed to the presence of other defects like Sn vacancies that lower the Fermi level. We will return to discuss this point by examining the electronic density of states later.

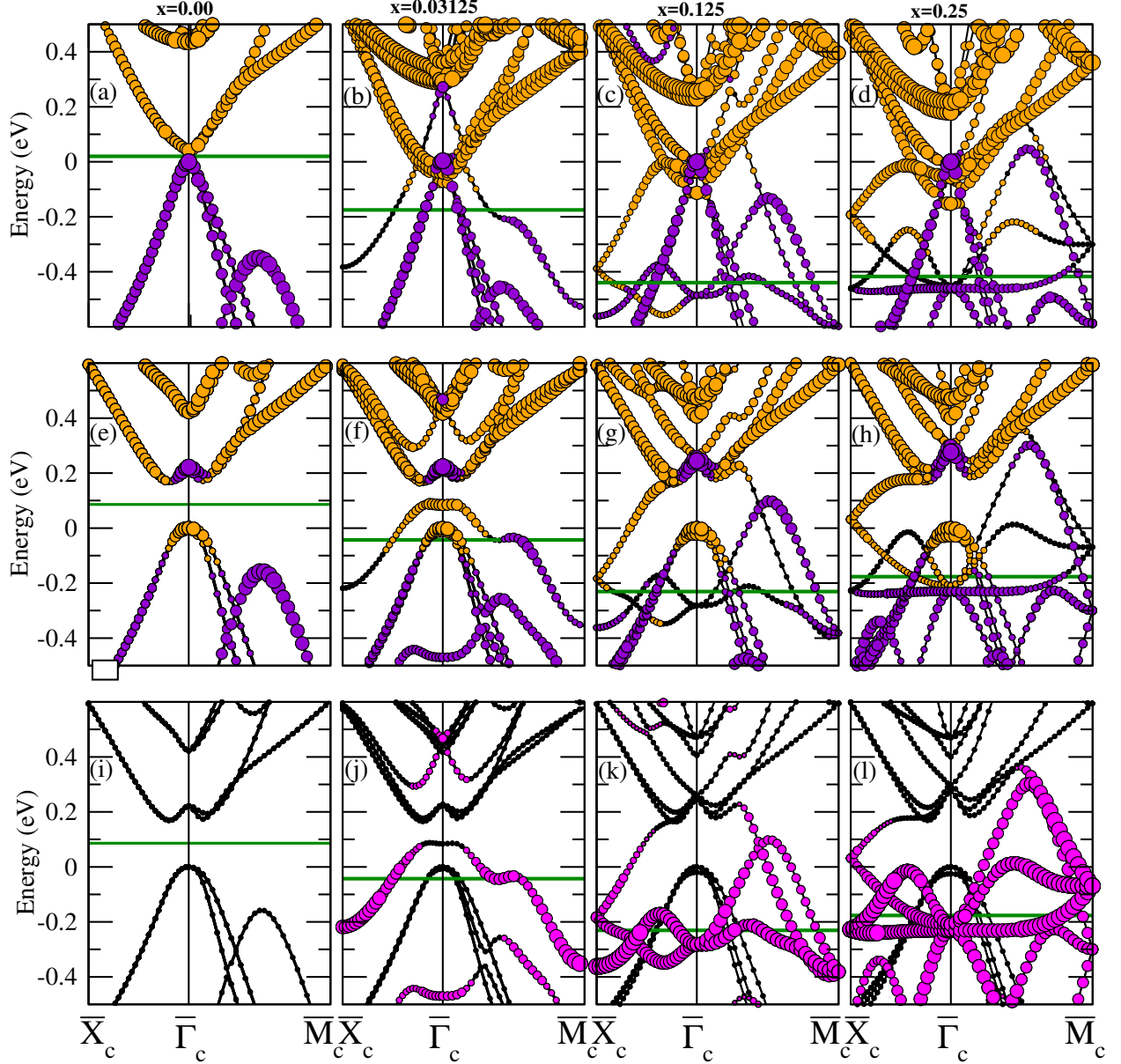


Figure 2: Band structure without SO coupling (top row (a)-(d)) and with SO (middle row (e)-(h)) showing the band inversion for the projected orbitals  $\Phi_+ = [\phi_P^{Te} + \phi_S^{Sn}]$  (in purple) and  $\Phi_- = [\phi_P^{Sn} + \phi_S^{Te}]$  (in orange). And bottom row (i)-(l) is the projection of In-5s electronic states of pristine SnTe,  $\text{Sn}_{0.96875}\text{In}_{0.03125}\text{Te}$ ,  $\text{Sn}_{0.175}\text{In}_{0.875}\text{Te}$ , and  $\text{Sn}_{0.75}\text{In}_{0.25}\text{Te}$ , respectively. The symbol sizes are proportional to the projection intensities. The horizontal green line is the Fermi level.

The p-orbitals of cation and anion has been used as a basis to compute the mirror Chern number for pristine SnTe [31], as well as IV-VI monolayers [46]. The p-orbitals of cations contributing to VBM and the p-orbitals of anions contributing to CBM, are all aligned along the [111] direction. This inverted orbital ordering produces a negative band gap. In Fig. 3 we show schematically the evolution of the VBM and CBM orbital characters when In ions are incorporated at Sn sites. We can still identify the  $\Phi_- = [\phi_P^{Sn} + \phi_S^{Te}]$  and  $\Phi_+ = [\phi_P^{Te} + \phi_S^{Sn}]$  for the VBM and CBM, respectively, but we have an additional In state which is always around the band gap region. The In contribution of this state is quite low at the L ( $\Gamma_t$ ) point but increases away from this point. Importantly, the In state keeps the same character as the VBM, whether it is inside the band gap or above the CBM. For low In concentration,  $x = 0.03125$ , the In state is located inside the band gap and its contribution is pure p-orbital ( $\Phi_-^{In}$ ) aligned along the [111] direction,

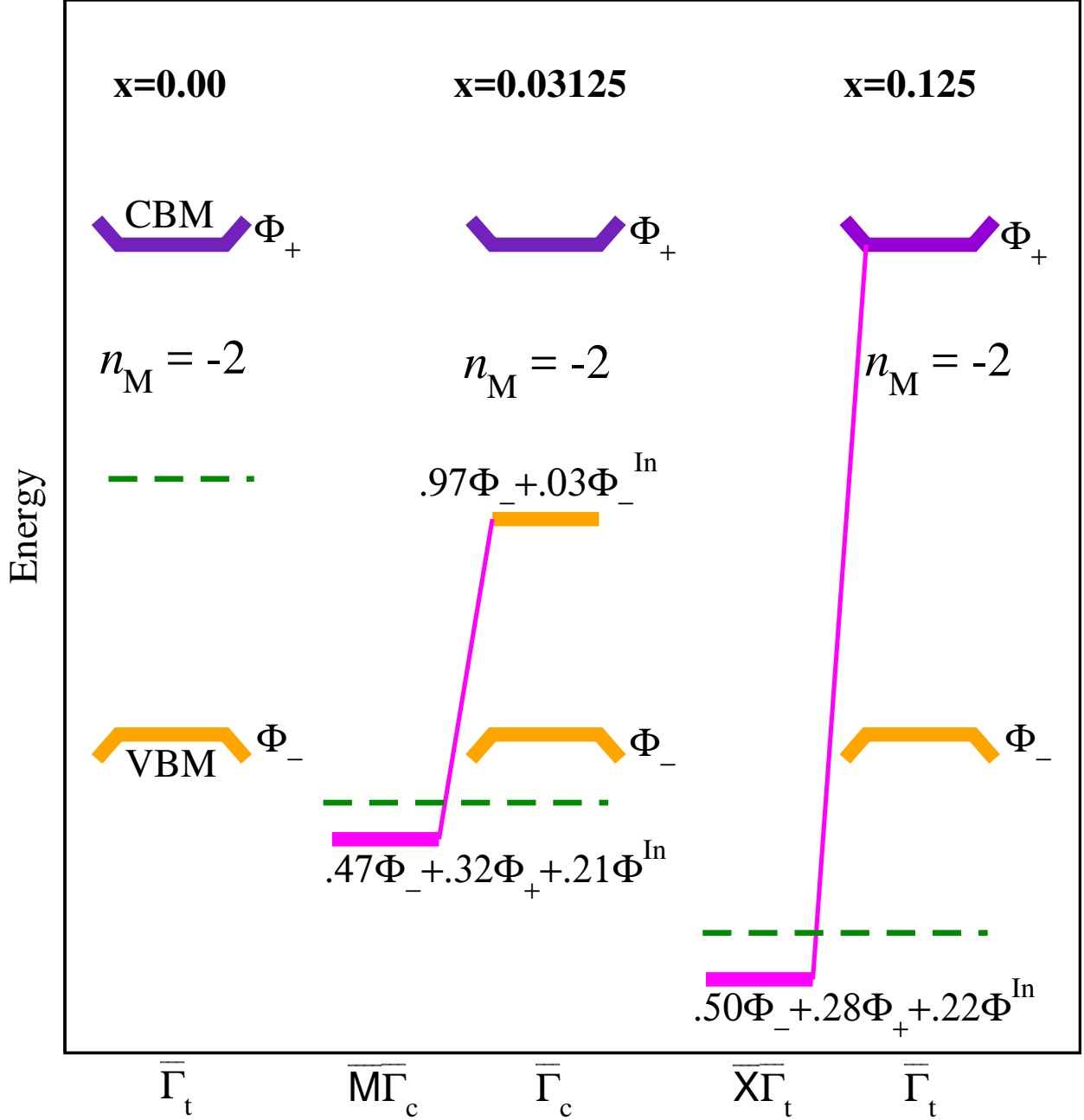


Figure 3: Schematic illustration of the computed orbital components of states in and around the band gap region for  $\text{Sn}_{1-x}\text{In}_x\text{Te}$ , with  $x = 0$ ,  $x = 0.03125$ , and  $x = 0.125$ . The  $\Phi_{\pm}$  states are explained in the text. The  $\Phi^{\text{In}}$  is a mixture of  $\Phi_{\pm}^{\text{In}}$ . The Fermi level is shown with green dashed lines.

the same character as that for the VBM cation Sn ion. As the gap is still inverted, the non-trivial topology is maintained. For high In concentration the In state is resonant inside the conduction band, and both VBM and CBM characters are the same as for the pristine one. Using the same procedure as described above the computed mirror Chern number for each of  $x = 0.03125$  and  $0.25$  is  $n_M = -2$ .

### 3.2 Topological Surface States

In the previous sub-section we have clearly verified the band inversion and non-trivial topological characteristics of pristine SnTe and  $\text{Sn}_{1-x}\text{In}_x\text{Te}$ . In a recent experimental study, using ARPES measurements, Sato *et al* [21] reported the existence of topological surface states, leading to the possibility of topological superconductivity in  $\text{Sn}_{1-x}\text{In}_x\text{Te}$ . In order to clarify the topological nature, we also performed calculations with a repeated slab geometry for pristine ( $x = 0$ ) and In doped system containing a low ( $x = 0.03125$ ) and a higher In doped concentration ( $x = 0.125$ ). Details of the slab makeup, including number of atomic layers and vacuum region, have been presented earlier. The mirror symmetry has been maintained for each slab geometry. However, substitutional In impurity breaks the top and bottom surface symmetries, yielding a reduction in the hybridization between the topological states of opposite surfaces.

Expressing, with respect to the mirror plane, symmetric and antisymmetric real space parts of wavefunction as  $|s\rangle$  and  $|a\rangle$ , respectively, and the spinor as  $|\sigma\rangle$ , the mirror eigenvalue equations can be stated as

$$\mathcal{M}|s, \pm\sigma\rangle = \pm i|s, \pm\sigma\rangle; \quad \mathcal{M}|a, \pm\sigma\rangle = \mp i|a, \pm\sigma\rangle.$$

This allows for two sets of topological surface states to be realized: the state  $(|s, \sigma\rangle + |a, -\sigma\rangle)$  corresponding to the eigenvalue  $+i$  and the state  $(|s, -\sigma\rangle + |a, \sigma\rangle)$  corresponding to the eigenvalue  $-i$ . Panel (a) in Fig. 4 shows the band structure of the pristine ( $x = 0$ ) SnTe slab geometry. The bulk band structure projected on to the tetragonal slab BZ is shown as shaded region. Consistent with the mirror symmetry and band inversion, a pair of surface bands corresponding to the mirror eigenvalues  $\pm i$  inside the bulk band gap region are identified (and shown in blue and red colors) extending along the  $\bar{\Gamma}_t\text{-}\bar{X}_t$  direction of the tetragonal BZ. The tiny band gap (around 36 meV) between the two surface bands in the middle of the bulk band gap, instead of Dirac crossing, is due to the interaction between the top and bottom surfaces of the slab. We also clearly identify a surface state (non topological origin) lying at around  $E_F - 0.17$  eV for part of the  $\bar{\Gamma}_t\text{-}\bar{X}_t$  direction.

As we can see in panels (b) and (c) of Fig. 4, topological surface states are present for both the low ( $x = 0.03125$ ) and high ( $x = 0.125$ ) In concentration regimes. The mirror symmetry is preserved for both In concentrations, as required for the presence of symmetry protected surface states. It is interesting to note that the topological state branch (blue color) coming from the valence band has contributions from In orbitals (pink color), while the topological state coming from the conduction band (red color) has pure SnTe character, similar to the pristine case in panel (a).

In a previous work in TCI [47] it was found that, as the slab thickness increases the interaction between top and bottom topological surface states reduces, leading to a reduction in the surface states band gap. We find that the surface state gaps for both  $x = 0.03125$  and  $x = 0.125$  are smaller than that for  $x = 0$ . Since the pristine SnTe slab, and the slab for  $x = 0.03125$  have the same thickness, we conclude that the presence of In impurity further reduces the surface band gap. The presence of substitutional In breaks the top and bottom surface symmetries, yielding a reduction of the hybridization between the topological states of opposite surfaces. Our work reveals that Indium doping of SnTe shifts the Dirac crossing energy position and also affects the Fermi velocities of the topological surface states. The main changes occur for topological hole states. As the doping moves the Fermi level downwards, the Fermi velocity increases with respect to the pristine system.

In Table I we summarise the topological surface state parameters for  $\text{Sn}_{1-x}\text{In}_x\text{Te}$ . For pristine SnTe, the Dirac crossing point is identified at a location with wavenumber  $k_D(L)$  away from the bulk L point. For  $\text{Sn}_{1-x}\text{In}_x\text{Te}$  the Dirac crossing point moves further way from the L point as  $x$  increases. The Fermi wavenumber  $k_F$  also increases as  $x$  increases. Our computed values of  $k_F$  are similar to the values reported in experimental works [29, 33], *albeit* for different  $x$  values and different surfaces. The electron and hole velocities have been computed in a range of 0.2 eV above and below the Dirac crossing point. The electron velocity,  $v_e$ , is almost independent of the  $x$  values. It is found that the hole velocity,  $v_h$ , has increased significantly for  $x = 0.125$ . In contrast, the Fermi velocity of the topological states,  $v_F$ , increases steadily with increase in  $x$ . Our computed Fermi velocities are in reasonable agreement with those obtained from quantum oscillation and ARPES measurements [29, 33]. In particular, the increase in  $v_F$  with increase in  $x$  has also been revealed from the ARPES measurements in [33] for  $x = 0.23$  and  $x = 0.41$  for the  $\text{Sn}_{1-x}\text{In}_x\text{Te}(111)$  surface.

We have estimated the Dirac crossing point to lie at 220 meV and 380 meV above the Fermi level for  $x = 0.03125$  and  $x = 0.125$ , respectively. The relative increase in  $E_D - E_F$  with increase in  $x$  has also been reported in [33] from a quantitative analysis of the ARPES spectrum for the (111) surface with  $x = 0.23$  and  $x = 0.41$ . Bulk states are always inside the topological surface bands, *i.e.* with  $k(\text{bulk}) < k_D(\text{surf})$ . This is consistent with the analysis of the ARPES study in [33] for their  $x = 0.23$  and  $x = 0.41$  samples.

### 3.3 Superconductivity Character

Transport, magnetization, and heat capacity measurements show that In substitution at Sn sites turns the TCI SnTe into a superconductor [22]. The superconductivity character of bulk  $\text{Sn}_x\text{In}_{1-x}\text{Te}$  can also be qualitatively analysed

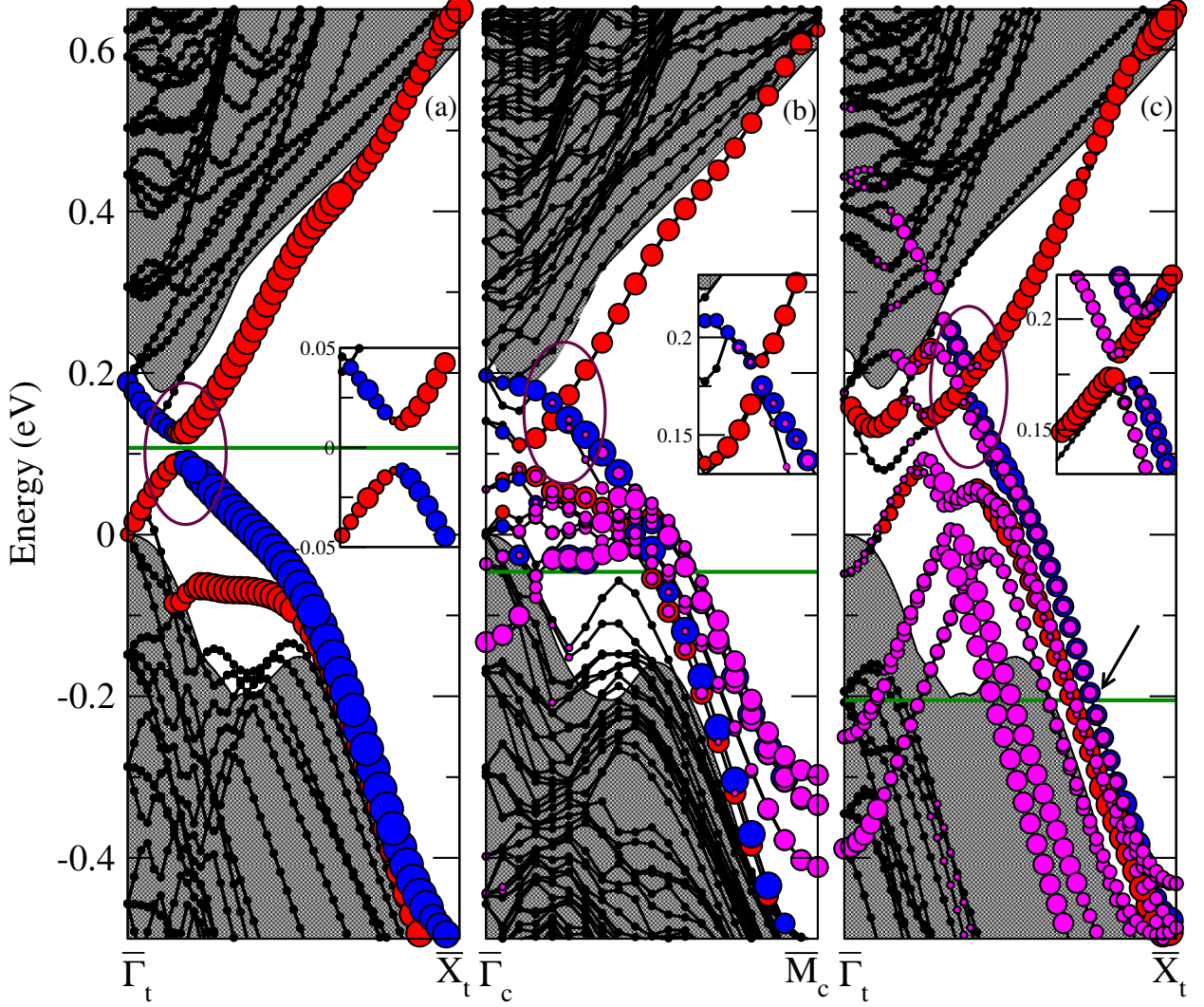


Figure 4: Topological surface states for  $\text{Sn}_{1-x}\text{In}_x\text{Te}$ : (a)  $x = 0$  (pristine  $\text{SnTe}$ ); (b)  $x = 0.03125$ ; (c)  $x = 0.125$ . Blue and red symbols represent the mirror eigenvalues  $+i$  and  $-i$  projected in half of the slab cell for bands around the valence and conduction band edges. The pink are the In-5s projected bands. The horizontal green line is the Fermi level. The back shadow region is the bulk projected band. The insets show magnified versions around the Dirac crossing region.

from our first principles calculations. The electronic density of states distribution near the Fermi level,  $DOS(E_F)$ , plays a dominant role in forming the BCS type superconducting state. According to the BCS theory, the formation energy of a Cooper pair increases linearly with  $DOS(E_F)$  [48]. With this in mind, in Fig. 5 we project the total and In contribution to the density of states. Comparing the results for  $x = 0$  (pristine  $\text{SnTe}$ ) and the low In concentration of  $x = 0.03125$  we find that there is a clear development of  $DOS(E_F)$  for the latter case. There is a progressively larger development of  $DOS(E_F)$  for the larger values of  $x = 0.125$  and  $x = 0.25$ . Our computed density of states per unit cell at the Fermi level for the three doping concentrations are 0.19, 0.73 and 0.78 states/eV for  $x = 0.03125$ ,  $x = 0.125$  and  $x = 0.25$ , respectively. These values are in quite good agreement with the estimated density of states based on magnetic susceptibility data [26] of 0.44 and 1.17 states/eV for  $x = 0.05$  and  $x = 0.40$ , respectively. For each of the three  $x$  values In-5s orbitals make almost the total contribution towards  $DOS(E_F)$ . Our results thus support a s-wave superconductivity in  $\text{Sn}_x\text{In}_{1-x}\text{Te}$ , in agreement with recent experimental observations [23, 24, 25, 27, 28]. We observe also from Fig. 5 that the In-5s orbital becomes less occupied for higher In doping regime, which prompts the  $p-$  to  $n-$  type transition as a function of increasing In concentration, providing support to the analysis of experimental measurements in [26, 29].

Table 1: Topological surface state parameters:  $k_D(L)$  is the Dirac crossing shift with respect to the pristine L point, Fermi wavenumber  $k_F$ , electron velocity  $v_e$ , hole velocity  $v_h$ , and Fermi velocity  $v_F$ . Wavenumbers in units of  $\text{\AA}^{-1}$ , and the velocities are in units of m/s.

	Pristine	$x = 0.03125$	$x = 0.125$	Experimental reports ( $x$ in the range 0.23-0.41)
$k_D(L)$	0.056	0.077	0.121	
$k_F$	0.000	0.101	0.131	0.04[29], 0.06-0.10[33]
$v_e$	3.02	3.03	2.76	
$v_h$	1.85	1.82	3.86	
$v_F$	2.46	3.56	5.79	2.5[29], 5.8-6.0[33]

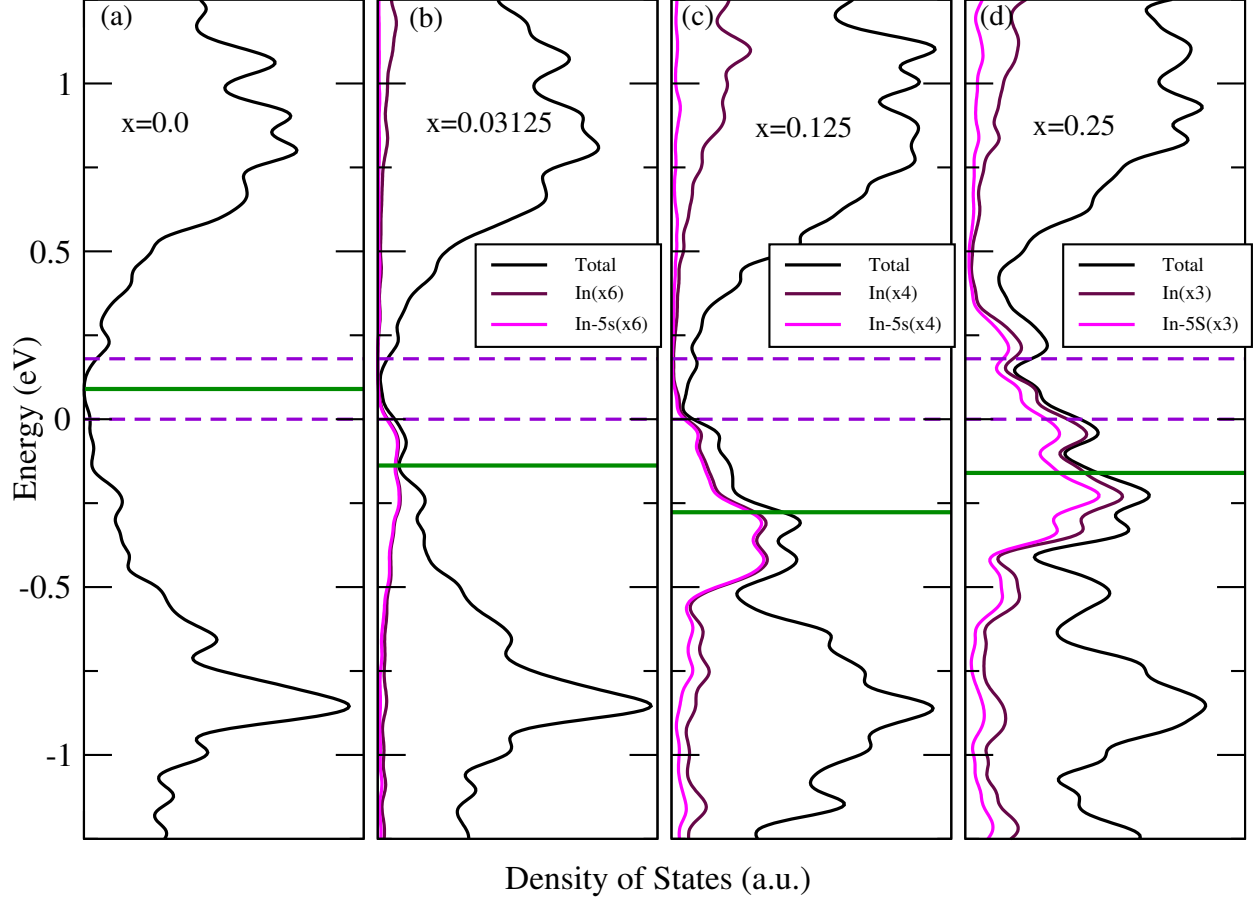


Figure 5: Total density of states (black) and local density of states projected on In (maroon) and on In-5s orbital (pink). The horizontal solid (green) line is the Fermi energy, and the dashed (violet) lines are the valence and conduction band edges.

## 4 Conclusion

We report on the non-trivial topological properties of the superconductor  $\text{Sn}_{1-x}\text{In}_x\text{Te}$ . The band inversion characteristic, *viz.* swapping of the normal contributions from p-anion and s-cation orbitals for the valence and conduction band edges (VBM and CBM), has been identified to arise in the presence of spin-orbit interaction. This inversion is preserved for In content systems with  $x = 0.03125, 0.125$  and  $0.25$ . The non-trivial phase has been confirmed by computing the mirror Chern number which is non-null for all those In concentrations. Topological states with opposite  $\pm i$  mirror eigenvalues has been identified on the (001) surface of the  $\text{Sn}_{1-x}\text{In}_x\text{Te}$ . With increase in In concentration, the location of the surface Dirac crossing point shifts progressively towards larger wavenumber. Also, the doping moves the Fermi

level downwards and the Fermi velocity progressively and significantly increases as  $x$  increases. We also verified that the density of states at the Fermi level for finite  $x$  values has been found to come mostly from In 5s orbitals. This confirms the  $s$ -wave nature of the superconducting state in agreement with some experimental studies. The results presented in this work demonstrate a non-trivial topological phase for the superconductor  $\text{Sn}_{1-x}\text{In}_x\text{Te}$ , and provide a detailed description of the topological state properties.

## Acknowledgements

One of the authors (TMS) acknowledge the financial support from the Brazilian Agencies INCT in Carbon Nanomaterials, CNPq, CAPES, FAPEMIG, and the computational facilities of LNCC and Cenapad.

## References

- [1] M. Z. Hasan and C. L. Kane. Colloquium: Topological insulators. *Rev. Mod. Phys.*, 82:3045–3067, Nov 2010.
- [2] Yoichi Ando. Topological insulator materials. *J. Phys. Soc. Jap.*, 82(10):102001, 2013.
- [3] Xiao-Liang Qi and Shou-Cheng Zhang. Topological insulators and superconductors. *Rev. Mod. Phys.*, 83:1057–1110, Oct 2011.
- [4] Yoichi Ando and Liang Fu. Topological crystalline insulators and topological superconductors: From concepts to materials. *Annu. Rev. Condens. Matter Phys.*, 6(1):361–381, 2015.
- [5] Masatoshi Sato and Yoichi Ando. Topological superconductors: a review. *Rep. Prog. Phys.*, 80(1):076501, 2017.
- [6] Charles L Kane and Eugene J Mele.  $\mathbb{Z}_2$  topological order and the quantum spin Hall effect. *Phys. Rev. Lett.*, 95(14):146802, 2005.
- [7] Liang Fu. Topological crystalline insulators. *Phys. Rev. Lett.*, 106(10):106802, 2011.
- [8] Liang Fu and C. L. Kane. Superconducting proximity effect and majorana fermions at the surface of a topological insulator. *Phys. Rev. Lett.*, 100:096407, Mar 2008.
- [9] S.-Y. Xu, N. Alidoust, I. Belopolski, A. Richardella, C. Liu, M. Newpene, G. Bian, S. H. Huang, R. Sankar, C. Fang, B. Dellabetta, W. Dai, Q. Li, M. J. Gilbert, F. Chou, N. Samarth, and M. Hasan. Momentum-space imaging of Cooper pairing in a half-Dirac-gas topological superconductor. *Nature Phys.*, (10):943, 2014.
- [10] Y. S. Hor, A. J. Williams, J. G. Checkelsky, P. Roushan, J. Seo, Q. Xu, H. W. Zandbergen, A. Yazdani, N. P. Ong, and R. J. Cava. Superconductivity in  $\text{Cu}_x\text{Bi}_2\text{Se}_3$  and its implications for pairing in the undoped topological insulator. *Phys. Rev. Lett.*, 104:057001, Feb 2010.
- [11] M. Kriener, Kouji Segawa, Zhi Ren, Satoshi Sasaki, and Yoichi Ando. Bulk superconducting phase with a full energy gap in the doped topological insulator  $\text{Cu}_x\text{Bi}_2\text{Se}_3$ . *Phys. Rev. Lett.*, 106:127004, Mar 2011.
- [12] M. Kriener, Kouji Segawa, Zhi Ren, Satoshi Sasaki, Shohei Wada, Susumu Kuwabata, and Yoichi Ando. Electrochemical synthesis and superconducting phase diagram of  $\text{Cu}_x\text{Bi}_2\text{Se}_3$ . *Phys. Rev. B*, 84:054513, Aug 2011.
- [13] Pradip Das, Yusuke Suzuki, Masashi Tachiki, and Kazuo Kadowaki. Spin-triplet vortex state in the topological superconductor  $\text{Cu}_x\text{Bi}_2\text{Se}_3$ . *Phys. Rev. B*, 83:220513(R), Jun 2011.
- [14] Zhongheng Liu, Xiong Yao, Jifeng Shao, Ming Zuo, Li Pi, Shun Tan, Changjin Zhang, and Yuheng Zhang. Superconductivity with topological surface state in  $\text{Sr}_x\text{Bi}_2\text{Se}_3$ . *J. Am. Chem. Soc.*, 137(33):10512–10515, 2015.
- [15] Shruti, V. K. Maurya, P. Neha, P. Srivastava, and S. Patnaik. Superconductivity by Sr intercalation in the layered topological insulator  $\text{Bi}_2\text{Se}_3$ . *Phys. Rev. B*, 92:020506(R), Jul 2015.
- [16] J. A. Schneeloch, R. D. Zhong, Z. J. Xu, G. D. Gu, and J. M. Tranquada. Dependence of superconductivity in  $\text{Cu}_x\text{Bi}_2\text{Se}_3$  on quenching conditions. *Phys. Rev. B*, 91:144506, Apr 2015.
- [17] M. P. Smylie, H. Claus, U. Welp, W.-K. Kwok, Y. Qiu, Y. S. Hor, and A. Snezhko. Evidence of nodes in the order parameter of the superconducting doped topological insulator  $\text{Nb}_x\text{Bi}_2\text{Se}_3$  via penetration depth measurements. *Phys. Rev. B*, 94:180510(R), Nov 2016.
- [18] Zhiwei Wang, A. A. Taskin, Tobias Frölich, Markus Braden, and Yoichi Ando. Superconductivity in  $\text{Te}_{0.6}\text{Bi}_{1.4}\text{Te}_3$  derived from a topological insulator. *Chem. Mat.*, 28(3):779–784, 2016.
- [19] Satoshi Sasaki, Zhi Ren, A. A. Taskin, Kouji Segawa, Liang Fu, and Yoichi Ando. Odd-parity pairing and topological superconductivity in a strongly spin-orbit coupled semiconductor. *Phys. Rev. Lett.*, 109:217004, Nov 2012.

- [20] A. S. Erickson, J.-H. Chu, M. F. Toney, T. H. Geballe, and I. R. Fisher. Enhanced superconducting pairing interaction in indium-doped tin telluride. *Phys. Rev. B*, 79:024520, Jan 2009.
- [21] T. Sato, Y. Tanaka, K. Nakayama, S. Souma, T. Takahashi, S. Sasaki, Z. Ren, A. A. Taskin, Kouji Segawa, and Yoichi Ando. Fermiology of the strongly spin-orbit coupled superconductor  $\text{sn}_{1-x}\text{in}_x\text{Te}$ : Implications for topological superconductivity. *Phys. Rev. Lett.*, 110:206804, May 2013.
- [22] G. Balakrishnan, L. Bawden, S. Cavendish, and M. R. Lees. Superconducting properties of the in-substituted topological crystalline insulator  $\text{snTe}$ . *Phys. Rev. B*, 87:140507(R), Apr 2013.
- [23] V. K. Maurya, Shruti, P. Srivastava, and S. Patnaik. Superconducting properties of indium-doped topological crystalline insulator  $\text{snTe}$ . *Europhys. Lett.*, 108(3):37010, 2014.
- [24] M. Saghiri, J. A. T. Barker, G. Balakrishnan, A. D. Hillier, and M. R. Lees. Superconducting properties of  $\text{sn}_{1-x}\text{in}_x\text{Te}$  ( $x = 0.38 - 0.45$ ) studied using muon-spin spectroscopy. *Phys. Rev. B*, 90:064508, Aug 2014.
- [25] Jie Shen, Yujun Xie, and Judy J. Cha. Revealing surface states in in-doped  $\text{snTe}$  nanoplates with low bulk mobility. *Nano Lett.*, 15(6):3827–3832, 2015.
- [26] Neel Haldolaarachchige, Quinn Gibson, Weiwei Xie, Morten Bormann Nielsen, Satya Kushwaha, and R. J. Cava. Anomalous composition dependence of the superconductivity in in-doped  $\text{snTe}$ . *Phys. Rev. B*, 93:024520, Jan 2016.
- [27] Satoki Maeda, Ryohei Hirose, Kazuaki Matano, Mario Novak, Yoichi Ando, and Guo-qing Zheng. Spin-singlet superconductivity in the doped topological crystalline insulator  $\text{sn}_{0.96}\text{in}_{0.04}\text{Te}$ . *Phys. Rev. B*, 96:104502, Sep 2017.
- [28] M. P. Smylie, H. Claus, W.-K. Kwok, E. R. Loudon, M. R. Eskildsen, A. S. Sefat, R. D. Zhong, J. Schneeloch, G. D. Gu, E. Bokari, P. M. Niraula, A. Kayani, C. D. Dewhurst, A. Snezhko, and U. Welp. Superconductivity, pairing symmetry, and disorder in the doped topological insulator  $\text{sn}_{1-x}\text{in}_x\text{Te}$  for  $x \geq 0.10$ . *Phys. Rev. B*, 97:024511, Jan 2018.
- [29] Cheng Zhang, Xu-Gang He, Hang Chi, Ruidan Zhong, Wei Ku, Genda Gu, J. M. Tranquada, and Qiang Li. Electron and hole contributions to normal-state transport in the superconducting system  $\text{sn}_{1-x}\text{in}_x\text{Te}$ . *Phys. Rev. B*, 98:054503, Aug 2018.
- [30] Kejing Ran, Ruidan Zhong, Tong Chen, Yuan Gan, Jinghui Wang, B. L. Winn, A. D. Christianson, Shichao Li, Zhen Ma, Song Bao, Zhengwei Cai, Guangyong Xu, J. M. Tranquada, Genda Gu, Jian Sun, and Jinsheng Wen. Unusual phonon density of states and response to the superconducting transition in the in-doped topological crystalline insulator  $\text{pb}_{0.5}\text{sn}_{0.5}\text{Te}$ . *Phys. Rev. B*, 97:220502(R), Jun 2018.
- [31] Timothy H Hsieh, Hsin Lin, Junwei Liu, Wenhui Duan, Arun Bansil, and Liang Fu. Topological crystalline insulators in the SnTe material class. *Nature communications*, 3:982, 2012.
- [32] Y Tanaka, Zhi Ren, T Sato, K Nakayama, S Souma, T Takahashi, Kouji Segawa, and Yoichi Ando. Experimental realization of a topological crystalline insulator in SnTe. *Nature Physics*, 8(11):800–803, 2012.
- [33] C. M. Polley, V. Jovic, T.-Y. Su, M. Saghiri, D. Newby, B. J. Kowalski, R. Jakiela, A. Barcz, M. Guziewicz, T. Balasubramanian, G. Balakrishnan, J. Laverock, and K. E. Smith. Observation of surface states on heavily indium-doped  $\text{snTe}(111)$ , a superconducting topological crystalline insulator. *Phys. Rev. B*, 93:075132, Feb 2016.
- [34] Alexey A. Soluyanov and David Vanderbilt. Computing topological invariants without inversion symmetry. *Phys. Rev. B*, 83:235401, Jun 2011.
- [35] Dominik Gresch, Gabriel Autès, Oleg V. Yazyev, Matthias Troyer, David Vanderbilt, B. Andrei Bernevig, and Alexey A. Soluyanov. Z2pack: Numerical implementation of hybrid wannier centers for identifying topological materials. *Phys. Rev. B*, 95:075146, Feb 2017.
- [36] John P. Perdew, Kieron Burke, and Matthias Ernzerhof. Generalized gradient approximation made simple. *Phys. Rev. Lett.*, 77:3865–3868, Oct 1996.
- [37] P. E. Blöchl. Projector augmented-wave method. *Phys. Rev. B*, 50:17953–17979, Dec 1994.
- [38] G. Kresse and J. Furthmüller. Efficiency of ab-initio total energy calculations for metals and semiconductors using a plane-wave basis set. *Comp. Mat. Sci.*, 6(1):15 – 50, 1996.
- [39] G. Kresse and J. Furthmüller. Efficient iterative schemes for ab initio total-energy calculations using a plane-wave basis set. *Phys. Rev. B*, 54:11169–11186, Oct 1996.
- [40] Paolo Giannozzi, Stefano Baroni, Nicola Bonini, Matteo Calandra, Roberto Car, Carlo Cavazzoni, Davide Ceresoli, Guido L Chiarotti, Matteo Cococcioni, Ismaila Dabo, Andrea Dal Corso, Stefano de Gironcoli, Stefano Fabris, Guido Fratesi, Ralph Gebauer, Uwe Gerstmann, Christos Gougoussis, Anton Kokalj, Michele Lazzeri, Layla

- Martin-Samos, Nicola Marzari, Francesco Mauri, Riccardo Mazzarello, Stefano Paolini, Alfredo Pasquarello, Lorenzo Paulatto, Carlo Sbraccia, Sandro Scandolo, Gabriele Sclauzero, Ari P Seitsonen, Alexander Smogunov, Paolo Umari, and Renata M Wentzcovitch. Quantum espresso: a modular and open-source software project for quantum simulations of materials. *Journal of Physics: Condensed Matter*, 21(39):395502 (19pp), 2009.
- [41] Hendrik J. Monkhorst and James D. Pack. Special points for brillouin-zone integrations. *Phys. Rev. B*, 13:5188–5192, Jun 1976.
- [42] Y. W. Tsang and Marvin L. Cohen. Calculation of the temperature dependence of the energy gaps in pbte and snte. *Phys. Rev. B*, 3:1254–1261, Feb 1971.
- [43] John P. Walter and Marvin L. Cohen. Pseudopotential calculations of electronic charge densities in seven semiconductors. *Phys. Rev. B*, 4:1877–1892, Sep 1971.
- [44] T. P. Humphreys and G. P. Srivastava. Nonlocal pseudopotential calculations for two isoelectronic series: Ge-gaas-znse and  $\alpha$ -sn-insb-cdte. *physica status solidi (b)*, 112(2):581–597, 1982.
- [45] Nicola Marzari and David Vanderbilt. Maximally localized generalized wannier functions for composite energy bands. *Phys. Rev. B*, 56:12847–12865, Nov 1997.
- [46] Augusto L. Araújo, Ernesto O. Wrasse, Gerson J. Ferreira, and Tome M. Schmidt. Topological nonsymmorphic ribbons out of symmorphic bulk. *Phys. Rev. B*, 93:161101(R), Apr 2016.
- [47] Augusto L. Araújo, Gerson J. Ferreira, and Tome M. Schmidt. Supressed topological phase transitions due to nonsymmorphism in snte stacking. *Sci. Rep.*, 8:9452, Jun 2018.
- [48] J. M. Ziman. *Principles of the theory of solids*. Cambridge University Press, 1964.